ZKG INTERNATIONAL

ISSN: 2366-1313

Significance of Nanofluid on steady 2-D MHD radiative fluid flow along a stretching sheet in presence of Multiple Slips effects: A Numerical Study

P. Valsamy[1] ,S. Jana Reddy[2,*] and D. Srinivas Reddy[2]

[1]*Engineering Mathematics, Faculty of Engineering and Technology, Annamalai University Chidambaram, Tamilnadu, India.*
[2]*Department of Mathematics, Vardhaman College of Engineering, Hyderabad, Telangana State, India.*

[*]Corresponding author Email address: *sunki.janareddy@gmail.com*

Abstract: Investigations have been made into the two-dimensional flow of a non-Newtonian nanofluid in the presence of thermal radiation, velocity slip, thermal slip, and concentration slip effects. Studying the effects of heat radiation involves using the Roseland approximation, which is a component of the energy equation. The immediate effects of the energy and concentration of the nanoparticles have also been considered and discussed. By introducing conditions for velocity, temperature, and concentration slip, the investigation is made more engaging. We discuss the Brownian motion and thermophoresis effects in the flow conditions for nanofluids. Mathematical models are used to represent the laws of conservation of mass, momentum, energy, and mass fraction profiles. Quantitative computations are made, and the results are fully described using both pictures and numbers. Then, utilising past study, the numerical code is validated.

Keywords: MHD; Nanofluid; Multiple Slip effects; Thermal radiation; Prandtl number; RK-method;

Nomenclature:

List of Symbols:

u, v: Velocity components in x and y axes respectively (m/s)
x, y: Cartesian coordinates measured along the stretching sheet (m)
f: Dimensionless stream function ($kg/\ m.\ s$)
f': Fluid velocity (m/s)
$\Pr$: Prandtl number
C: Fluid nanoparticle volume concentration (mol/m^3)
C_∞: Dimensional ambient volume fraction (mol/m^3)
T: Fluid temperature (K)
T_w: Temperature at the surface (K)

Greek symbols:

B_o: Uniform magnetic field ($Tesla$)
q_m: Mass flux coefficient
T_∞: Temperature of the fluid far away from the stretching sheet (K)
O: Origin
C_w: Dimensional nanoparticle volume concentration at the stretching surface (mol/m^3)
M^2: Magnetic field parameter
Cf: Skin-friction coefficient (s^{-1})
Nu: Rate of heat transfer coefficient (or) Nusselt number
$u_w(x)$: Stretching velocity of the fluid (m/s)
Nb: Brownian motion parameter
Nt: Thermophoresis parameter
Le: Lewis number parameter
q_w: Heat flux coefficient
C_p: Nano particles Specific heat capacity ($J/kg/K$)
D_B: Coefficient of Brownian diffusion (m^2/s)

ISSN: 2366-1313

D_T : Coefficient of Thermophoresis diffusion (m^2 / s)
Sh : Rate of mass transfer coefficient (or) Sherwood number
a : A constant
K^* : Mean absorption coefficient
R : Thermal radiation parameter
q_r : Radiative heat flux
L_1 : Slip length (m)
L_2 : Thermal slip length (m)
L_3 : Concentration slip length (m)
Re_x : Reynolds number
η : Dimensionless similarity variable (m)
θ : Dimensionless temperature (K)
α : Thermal diffusivity (m^2/s)
ν : Kinematic viscosity (m^2/s)
ϕ : Dimensional nanoparticle volume concentration (mol/m^3)
σ : Stefan-Boltzmann constant
ρ : Fluid density (kg / m^3)
σ^* : Stefan-Boltzmann constant
λ : Velocity slip parameter
δ : Thermal slip parameter
λ : Concentration slip parameter
κ : Thermal conductivity ($W / (m \cdot K)$)
τ_w : Shear stress

Superscript:

$'$: Differentiation w.r.t η

Subscripts:

f : Fluid
w : Condition on the sheet
∞ : Ambient Conditions

1. Introduction:

In the solar sector, in particular, radiation is a kind of energy transmission that has a wide range of applications. No material medium is required for this kind of heat transmission. A number of academics have shown interest in heat radiation's effects, perhaps as a result of all the ways it has been used to make polymers. Furthermore, nano-liquids are thought to be among the most effective refrigerant liquids in sectors including transportation, microelectronics, optical, and manufactured products. Due to its many uses in power production, cooling nuclear reactors, and combustion, radiant heat transfer is essential. These affects mostly occurred in space ship re-entry, astrophysical flows, fossil fuel, solar power technologies, etc. when the difference between the surface and ambient temperatures was very significant. Designing creative energy conversion systems that are successful at high temperatures requires a solid understanding of the mechanisms involved in solar radiation. Activation energy, radiation, the double Cattaneo-Christov theory, and the Williamson nanofluid were all used by Tamilzharasan et al. [1] in their investigation. As a result of non-linear thermal radiation and slip effects, Bilal [2] investigated the characteristics of micropolar flow in electro-magnetohydrodynamic nanofluid flow. When studying the parameters of heat transmission using ferromagnetic hybrid nanofluid, Kumar et al. [3] took into account the impact of sun radiation. In a converging/diverging channel with Rosseland radiation present, Raza et al. [4] .'s study of MHD flow of non-Newtonian nanofluid. Two-dimensional MHD stagnation point flow, heat, and mass transfer across a porous medium were reported by Nandeppanavar et al. [5] owing to the influence of a porous stretched sheet and thermal radiation. Sreedevi et al. [6] .'s investigation on the combined impacts of heat and mass transfer study of an unstable hybrid nanofluid flow across a stretched sheet with thermal radiation. A cylinder-shaped Maxwell nano-liquid was used by

ISSN: 2366-1313

Chu et al. [7] to study Cattaneo-Christov and radiative heat flow. By using heat radiation and the Cattaneo-Christov flux, Mubaddel et al. [8] examined the bio-convection flow of Sisko nanoliquid. The effects of heat radiation and bio-convection on the axi-symmetric flow of Sutter by nanofluid with motile microorganisms were studied by Azam [9]. For cross nanofluid under the influence of nonlinear radiation and Lorentz forces, Azam et al. [10] developed mathematical models. An investigation into the effects of magnetic fields and solar radiation on Reiner-Philippoff nanofluid was published by Reddy et al. [11]. The Buongiorno's model was used by Sheikholeslami et al. [12] to study the flow of nanofluid across a flexible plate in the presence of a magnetic field and radiation heat transfer. Al-Mdallal et al. [13] .'s investigation of the motion of different hybrid nanofluids on a flat plate with Marangoni boundary conditions while subjected to radiation and an angled magnetic field looked at the impact on the flow of the fluids. In a rotating stretching channel with a fixed bottom wall and nonlinear thermal radiation, Ghadikolaei et al. [14] studied the three-dimensional MHD squeezing flow and heat transfer of (Fe3O4)-Ag/ethylene glycol-water hybrid nanoparticles. Ghadikolaei et al. [15] analysed a rotating channel with a fixed bottom wall and nonlinear thermal radiation. The impact of heat radiation on different disciplines was explored by several of the writers ([16]-[30]). The current study, which was inspired by the previously mentioned research literature, aims to investigate the combined effects of velocity, thermal, and concentration slips on steady, incompressible, viscous, non-Newtonian fluid flow in the presence of magnetic field and thermal radiation effects using the Runge-Kutta method. the following are the primary characteristics of this research work:

Using a stretched sheet and nanofluid, a novel numerical method for two-dimensional, laminar, steady magnetohydrodynamic flow has been developed. The effects of heat radiation and multiple slip effects have also been considered.

- Using appropriate similarity transformations, the fundamental governing equations in the form of PDEs are then condensed into the coupled non-linear ODEs.
- Implementing the R-K method thoroughly coupled with the shooting approach using MATLAB software is a revolutionary development that enables the completion of the necessary numerical solutions for such a challenge. A numerical solution approach called the R-K method, which is based on the shooting method, was created specifically to solve a group of very nonlinear O.D.Eqns.
- To continue and expand on the computational analysis for this work, the computational results are validated by comparing special cases of the present study.
- According to this theory, these variables have a big influence on lots of technical applications, such the production of polymers, metal layers, paper sheets, and biology.

2. Flow Governing Equations:

The multiple slips (velocity, thermal and concentration) effects on steady, two dimensional, viscous, incompressible, electrically conducting non-Newtonian nanofluid boundary layer flow towards a stretching sheet in presence of magnetic field, thermal radiation, thermophoresis and Brownian motion effects are studied in this research work. The flow geometry of this fluid flow is shown in Fig. 1. The following one by one assumptions are discussed for this investigation:

i. The non-linearly stretching sheet is stretched along x-direction and y-axis is normal to it.

ii. The nanofluid flow is occupied the domain $y > 0$.

iii. Generally, $B(x)$ a variable magnetic field will be provided to the surface of the sheet while the magnetic field induced is minimal and may be justified for MHD flow at the small magnetic Reynolds number.

iv. It is assumed that, the convective surface temperature is T_w and ambient temperature is T_∞.

v. Also, the concentration of the nano-particles at the sheet is C_w and ambient concentration is C_∞.

vi. Also, it is assumed that a homogeneous first order chemical reaction and thermal radiation are neglected in this flow.

ISSN: 2366-1313

vii. In addition, it is assumed that the effect described by Fourier's and Fick's law is of higher order of magnitude than the effect due to Dufour and Soret and thus the Dufour and Soret effects are neglected.

viii. Along *x*-direction, the velocity of the sheet is $u_w(x) = ax$ (1)

The fundamental governing equations for the conservations of mass, momentum, energy, and nanoparticles distribution for the nanofluid using the above assumptions with Boussinesq's and boundary-layer approximations, written as:

Continuity Equation:

$$\left(\frac{\partial u}{\partial x}\right)+\left(\frac{\partial v}{\partial y}\right)=0 \tag{2}$$

Momentum Equation:

$$u\left(\frac{\partial u}{\partial x}\right)+v\left(\frac{\partial u}{\partial y}\right)=\nu\left(\frac{\partial^2 u}{\partial y^2}\right)-\left(\frac{\sigma B_o^2}{\rho}\right)u \tag{3}$$

Equation of thermal energy:

$$u\left(\frac{\partial T}{\partial x}\right)+v\left(\frac{\partial T}{\partial y}\right)=\alpha\left(\frac{\partial^2 T}{\partial x^2}+\frac{\partial^2 T}{\partial y^2}\right)+\tau_B\left\{D_B\left[\left(\frac{\partial C}{\partial x}\right)\left(\frac{\partial T}{\partial x}\right)+\left(\frac{\partial C}{\partial y}\right)\left(\frac{\partial T}{\partial y}\right)\right]+\left(\frac{D_T}{T_\infty}\right)\left[\left(\frac{\partial T}{\partial x}\right)^2+\left(\frac{\partial T}{\partial y}\right)^2\right]\right\}$$

$$-\frac{1}{\rho C_p}\left(\frac{\partial q_r}{\partial y}\right) \tag{4}$$

Equation of species nanoparticle volume concentration:

$$u\left(\frac{\partial C}{\partial x}\right)+v\left(\frac{\partial C}{\partial y}\right)=D_B\left[\left(\frac{\partial^2 C}{\partial x^2}\right)+\left(\frac{\partial^2 C}{\partial y^2}\right)\right]+\left(\frac{D_T}{T_\infty}\right)\left[\left(\frac{\partial^2 T}{\partial x^2}\right)+\left(\frac{\partial^2 T}{\partial y^2}\right)\right] \tag{5}$$

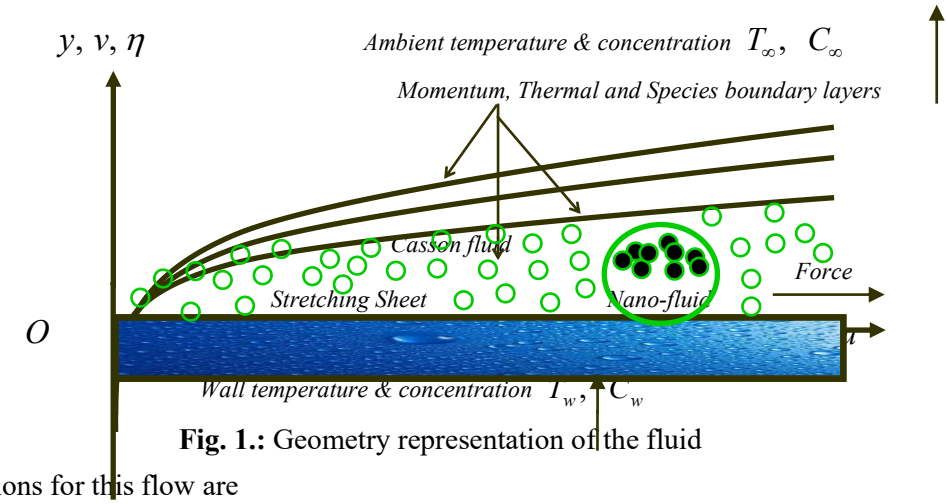

Fig. 1.: Geometry representation of the fluid

The boundary conditions for this flow are

$$\left.\begin{aligned} &u = u_w = ax + L_1\left(\frac{\partial u}{\partial y}\right),\ v = 0,\ T = T_w + L_2\left(\frac{\partial T}{\partial y}\right),\ C = C_w + L_3\left(\frac{\partial C}{\partial y}\right),\ at\ \ y = 0 \\ &u \to 0,\ T \to T_\infty,\ C \to C_\infty,\ \ as\ \ y \to \infty \end{aligned}\right\} \tag{6}$$

The radiative heat flux q_r (using Roseland approximation) is defined as

$$q_r = -\frac{4\sigma^*}{3K^*}\left(\frac{\partial T^4}{\partial y}\right) \tag{7}$$

We assume that the temperature variances inside the flow are such that the term T^4 can be represented as linear function of temperature. This is accomplished by expanding T^4 in a Taylor series about a free stream temperature T_∞ as follows:

$$T^4 = T_\infty^4 + 4T_\infty^3(T - T_\infty) + 6T_\infty^2(T - T_\infty)^2 + \ldots\ldots\ldots \tag{8}$$

ISSN: 2366-1313

After neglecting higher-order terms in the above equation beyond the first-degree term in $\left(T-T_\infty\right)$, we get

$$T^4 \cong 4T_\infty^3 T - 3T_\infty^4 \tag{9}$$

Thus substituting Eq. (9) in Eq. (8), we get

$$q_r = -\frac{16T_\infty^3\sigma^*}{3K^*}\left(\frac{\partial T}{\partial y}\right) \tag{10}$$

Using (10), Eq. (4) can be written as

$$u\left(\frac{\partial T}{\partial x}\right)+v\left(\frac{\partial T}{\partial y}\right)=\alpha\left(\frac{\partial^2 T}{\partial x^2}+\frac{\partial^2 T}{\partial y^2}\right)+\tau_B\left\{D_B\left[\left(\frac{\partial C}{\partial x}\right)\left(\frac{\partial T}{\partial x}\right)+\left(\frac{\partial C}{\partial y}\right)\left(\frac{\partial T}{\partial y}\right)\right]+\left(\frac{D_T}{T_\infty}\right)\left[\left(\frac{\partial T}{\partial x}\right)^2+\left(\frac{\partial T}{\partial y}\right)^2\right]\right\} \tag{11}$$

$$\frac{1}{\rho C_p}\left(\frac{16T_\infty^3\sigma^*}{3K^*}\right)\left(\frac{\partial^2 T}{\partial y^2}\right)$$

Introducing the following similarity transformations

$$\left.\begin{aligned} u = u_w f'(\eta),\ v = -\sqrt{\frac{\nu u_w}{x}}f(\eta),\ \eta = y\sqrt{\frac{u_w}{\nu x}},\ \theta = \frac{T-T_\infty}{T_w-T_\infty},\ \phi = \frac{C-C_\infty}{C_w-C_\infty} \end{aligned}\right\} \tag{12}$$

Making use of Eq. (12), equation of continuity is identically satisfied and Eqs. (3), (5) and (11) along with (6) take the following form

$$f'''(\eta)+f(\eta)f''(\eta)-M^2 f'(\eta)-2\left[f'(\eta)\right]^2=0 \tag{13}$$

$$\left(1+\frac{4}{3R}\right)\theta''(\eta)+\Pr f(\eta)\theta'(\eta)+\Pr Nb\theta'(\eta)\phi'(\eta)+\Pr Nt\left[\theta'(\eta)\right]^2=0 \tag{14}$$

$$Nb\phi''(\eta)+LeNb\Pr f(\eta)\phi'(\eta)+Nt\theta''(\eta)=0 \tag{15}$$

the corresponding boundary conditions (6) become

$$\left.\begin{aligned} f(\eta)=0,\ f'(\eta)=1+\lambda f''(\eta),\ \theta(\eta)=1+\delta\theta'(\eta),\ \phi(\eta)=1+\beta\phi'(\eta)\ at\ \eta=0 \\ f'(\eta)\to 0,\ \theta(\eta)\to 0,\ \phi(\eta)\to 0\ \ as\ \ \eta\to\infty \end{aligned}\right\} \tag{16}$$

where the involved physical parameters are defined as

$$\left.\begin{aligned} M^2=\frac{2\sigma B_o^2 L}{\rho U_o},\ \Pr=\frac{\nu}{\alpha},\ Le=\frac{\nu}{D_B},\ R=\frac{\kappa K^*}{4\sigma^* T_\infty^3},\ Nb=\frac{(\rho C)_p D_B(C_w-C_\infty)}{\nu(\rho C)_f}, \\ Nt=\frac{(\rho C)_p D_T(T_w-T_\infty)}{\nu T_\infty(\rho C)_f},\ \lambda=L_1\sqrt{\frac{a}{\nu}},\ \delta=L_2\sqrt{\frac{a}{\nu}},\ \beta=L_3\sqrt{\frac{a}{\nu}},\ \mathrm{Re}_x=\frac{u_w x}{\nu} \end{aligned}\right\} \tag{17}$$

Quantities of physical interest, the physical parameters of the skin-friction coefficient, local Nusselt number and local Sherwood number are presented as follows:

$$Cf_x=\frac{\tau_w}{\rho u_w}\Rightarrow Cf=\mathrm{Re}_x^{-\frac{1}{2}}Cf_x=f''(0) \tag{18}$$

$$Nu_x=\frac{xq_w}{\kappa(T_w-T_\infty)}\ \text{where}\ q_w=-k\left(\frac{\partial T}{\partial y}\right)_{y=0}+(q_r)_{y=0}\Rightarrow Nu=\mathrm{Re}_x^{-\frac{1}{2}}Nu_x=-\left(1+\frac{4}{3R}\right)\theta'(0) \tag{19}$$

$$Sh_x=\frac{xq_m}{D_B(T_w-T_\infty)}\ \text{where}\ q_m=-D_B\left(\frac{\partial C}{\partial y}\right)_{y=0}\Rightarrow Sh=\mathrm{Re}_x^{-\frac{1}{2}}Sh_x=-\phi'(0) \tag{20}$$

3. Method of Solution:

ISSN: 2366-1313

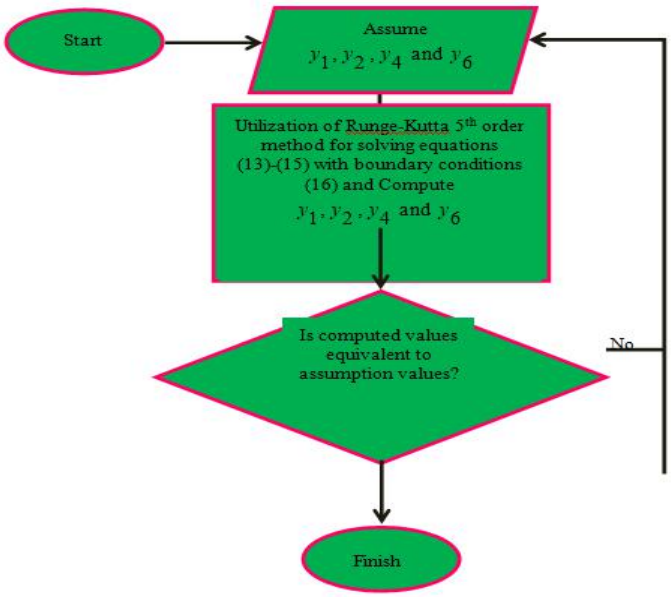

Fig. 2. The flow-chart of the present numerical method

In order to solve the nonlinear ODEs (13)-(15), the boundary conditions are required from (16). Maple is used to implement the fifth-order Runge-Kutta algorithm. The non-linear differential equations must first be turned into a system of first-order differential equations before they can be solved. New variables have been designed to do this:

$$f = y_1,\ f' = y_2,\ f'' = y_3,\ \theta = y_4,\ \theta' = y_5,\ \phi = y_6,\ \phi' = y_7\Big\} \tag{18}$$

The step size $\Delta\eta = 0.001$ is used to obtain the numerical solution with $\eta_{\max}$,with an accuracy to the fifth decimal place is chosen as the criterion of convergence. The asymptotic boundary conditions given by Eq. (16) were replaced by using a value similarity variable $\eta_{\max} = 8$ (for nanoparticle volume concentration profiles 10 and 12) as follows:

$$f'(\eta_{\max}) = 0,\ \ \theta(\eta_{\max}) = 0,\ \ \phi(\eta_{\max}) = 0 \tag{19}$$

The choice of $\eta_{\max} = 8$ (for nanoparticle volume concentration profiles 10 and 12) ensures that all numerical solutions approached the asymptotic values correctly.

4. Program Code Validation:

For program code validation, the authors have compared our numerical results with the published results of Wang [31], Reddy Gorla and Sidawi [32], Khan and Pop [33], and Makinde and Aziz [34] in table-1. From this table, the discrepancy between the two groups. They can construct a lot of things together since they have so much in common. Therefore, there is a high degree of trust in the simulations that have previously been developed.

Table-1.: Comparison of Nusselt number results with published Nusselt number results for variation of Prandtl number in absence of Nanofluid when $M = 0, \beta = 0, \delta = 0, R \to \infty$ & $\gamma = 0$

Pr	Wang [31]	Reddy Gorla and Sidawi [32]	Khan and Pop [33]	Makinde and Azaz [34]	Present numerical results
0.20	0.1691	0.1691	0.1691	0.1691	0.15992031556206489
0.70	0.4539	0.5349	0.4539	0.4539	0.44821717846602337
2.00	0.9114	0.9114	0.9113	0.9114	0.90586630044774566
7.00	1.8954	1.8905	1.8954	1.8954	1.88950014732644987

5. Results and Discussion:

The system of non-linear ordinary differential Eqs. (13), (14), (15) subjected to the boundary conditions (16) is

ISSN: 2366-1313

solved numerically by Runge-Kutta method along with shooting technique for the various values of physical engineering parameters such as M^2, λ, γ, β, Pr, R, Nb, Nt and Le. The results of flow variables such as velocity, temperature and nanoparticle concentration are discussed for variations of the above said parameters in figures 3, 4, 5, 6, 7, 8, 9, 10, 11, 12, 13. Also, the engineering quantities such as Skin-friction coefficient, Nusselt number and Sherwood number are discussed for the variations of above said parameters in tables 2, 3 and 4 respectively. Fig. 3 displays the impact of Magnetic field parameter (M^2) on the flow momentum. The velocity field and associated boundary layer drops down for negative inclusion of the magnetic effect in flow model. Physically, the stronger retardation and sudden bumps created by the magnetic field in the way of fluid motion are the reason behind this decline in fluid velocity. This retardation force is known as the Lorentz force effective normal to the fluid motion. The effect of velocity slip parameter (λ) on the velocity component distributions is demonstrated in Fig. 4. The velocity slip parameter varies from 0.5 to 2. The fluid velocity component reduces with increasing the values of velocity slip parameter. In other word, less amount of flow is drawn and pushed away in the velocity direction, as the slip gets stronger. This mentioned behaviour changes by crossing away from the stretching surface. This means that the velocity boundary- layer thickness becomes thicker for the larger amplitude of velocity slip parameter.

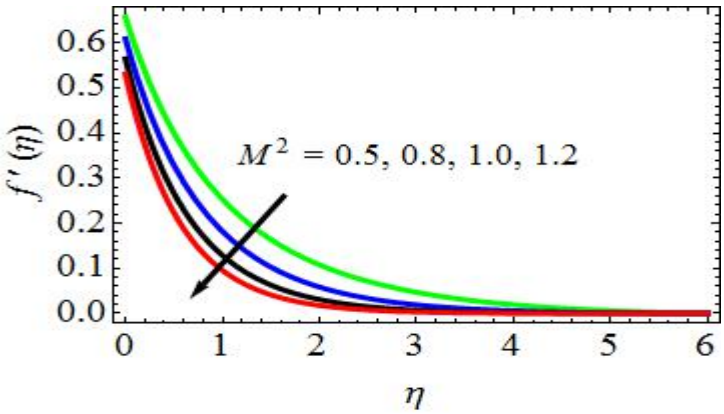

Fig. 3. Effect of M^2 on velocity profiles

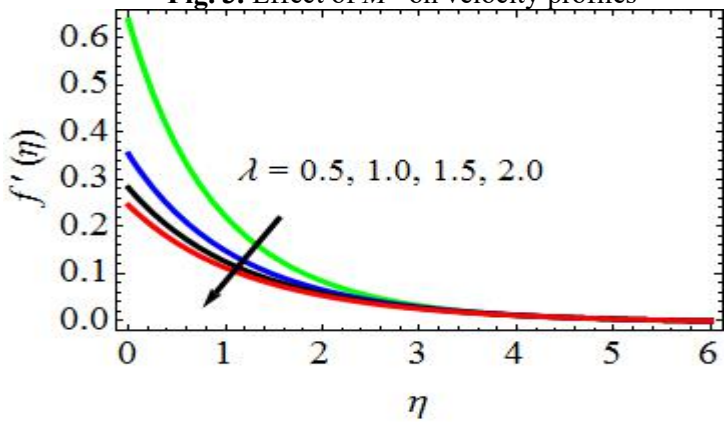

Fig. 4. Effect of λ on velocity profiles

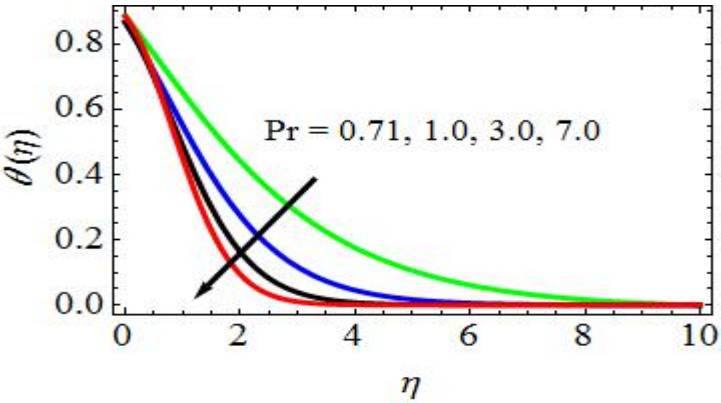

Fig. 5. Effect of Pr on temperature profiles

ISSN: 2366-1313

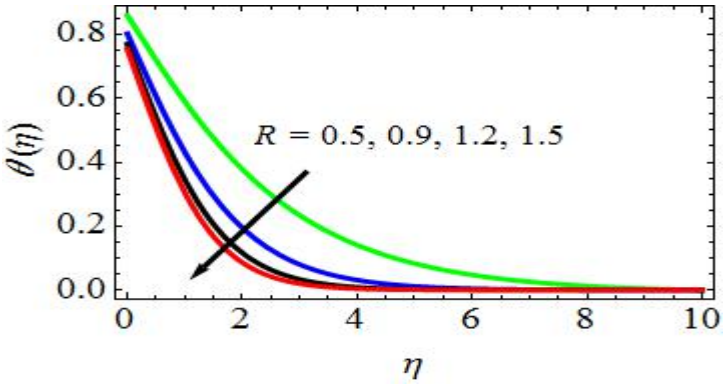

Fig. 6. Effect of *R* on temperature profiles

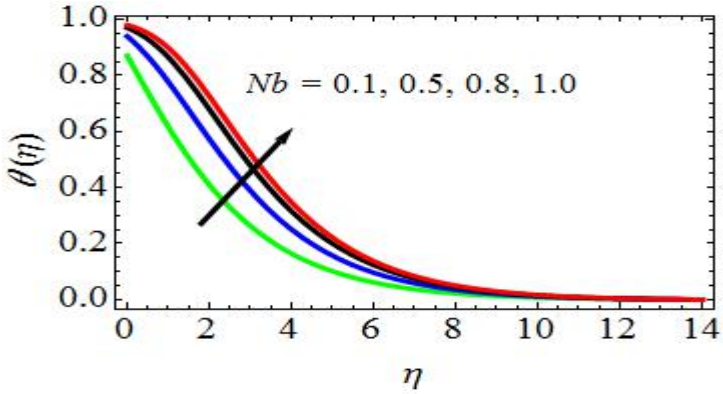

Fig. 7. Effect of *Nb* on temperature profiles

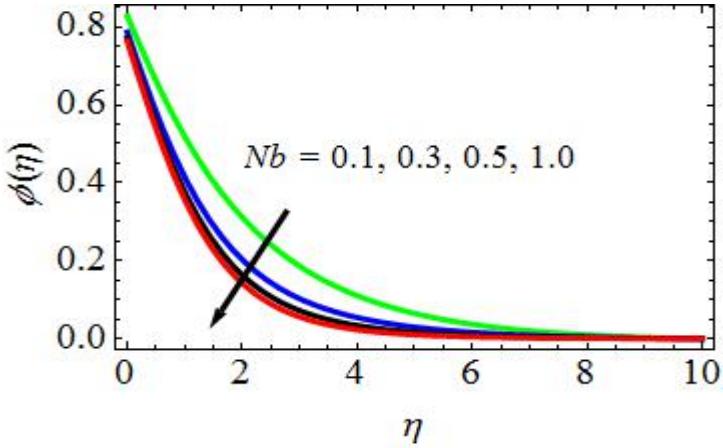

Fig. 8. Effect of *Nb* on concentration profiles

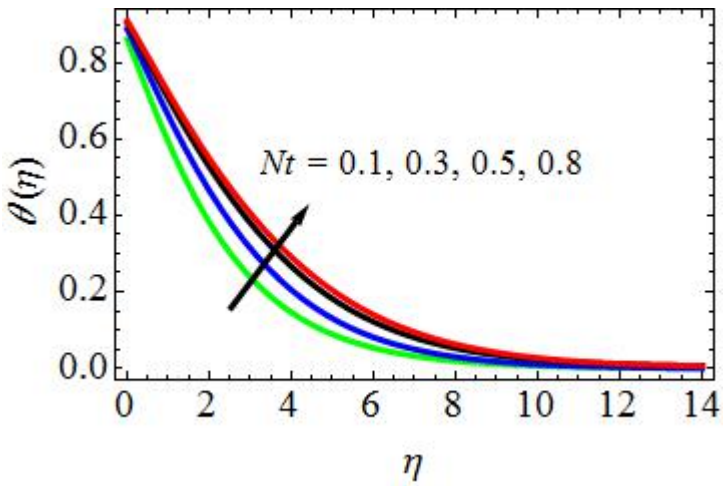

Fig. 9. Effect of *Nt* on temperature profiles

ISSN: 2366-1313

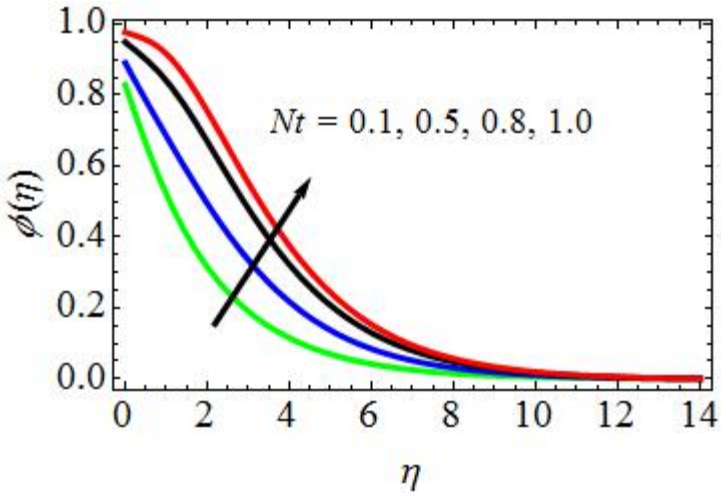

Fig. 10. Effect of *Nt* on concentration profiles

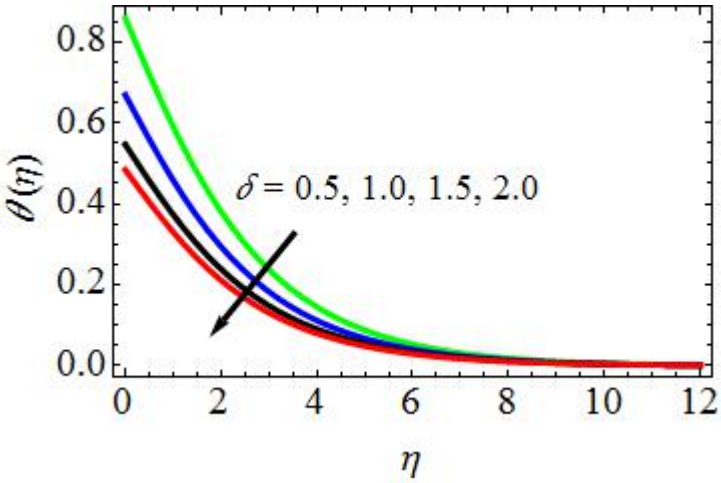

Fig. 11. Effect of δ on temperature profiles

Fig. 5 presents the effect of Prandtl number (Pr) on the fluid temperature. As the value of Pr increases, the temperature gradient of the fluid decreases. As Pr increases, the momentum diffusivity increases and dominates the thermal diffusivity. The fluid velocity is high enough to help the heat transfer of the fluid. This makes the heat dissipation rate faster and makes the boundary layer to become thinner. We can see in Fig. 11 that the thermal radiation parameter (*R*) has an influence on the temperature distribution $\theta(\eta)$ of the system. Heat dispersion increases when the thermal radiation parameter *R* is raised over its default value. As the value of *R* is raised, the thermal buoyancy force increases and the thickness of the thermal boundary layer decreases. On a physical level, increasing the thermal radiation parameter *R* causes more heat to be created in the fluid flow zone, resulting in more uniform temperature distributions $\theta(\eta)$. Fig. 7 shows that the temperature profiles and its corresponding boundary layer growth are substantially increased by the Brownian motion variable (*Nb*). In many nano-fluid flow problems, the existence of nanoparticles produces Brownian motion, and the Brownian motion (*Nb*) is influenced by the increase in Brownian motion (*Nb*). Fig. 8 illustrates the influences of Brownian motion parameter (*Nb*) on concentration profiles. As the effect of Brownian motion increases, the concentration gradient increases, and as a result, the Brownian force increase boots the nanoparticle concentration at the surface. Hence, the concentration profiles increase at the surface. Fig. 9 depicts the influence of Thermophoresis parameter (*Nt*) on temperature profiles. As the Thermophoretic effect increases, the migration of nanoparticles from the hot surface to cold ambient fluid is occurred, and as a result, the temperature increases in the boundary layer. This results in the growth of thermal boundary layer thickness. Fig. 10 shows the impact of Thermophoresis parameter (*Nt*) on concentration profiles. Since the impact of Brownian force is to counterbalance the influences of Thermophoretic force, as the influences of Thermophoretic force increase the concentration gradient at the surface decreases, as a result of this, the concentration profile at a surface decreases, which is opposite to the case for Brownian motion effect. Fig.11 exhibits the effect of the thermal slip parameter (δ) on the dimensionless temperature profiles. It is clearly shown that by

ISSN: 2366-1313

increasing the values of δ, the temperature profiles are decreases. As the value of the thermal slip parameter increases, the thermal boundary layer thickness decreases even when a small amount of heat is transferred to the fluid from the sheet. Fig. 12 depicts the influence of the Lewis number on the dimensionless nanoparticle volume concentration. It is noticed that the nanoparticle volume fraction experiences a strong reduction for larger *Le* values. The dimensionless Lewis number is defined as the ratio of thermal and mass diffusivity. By increasing the value of *Le*, the thermal boundary layer thickness is increased whereas the nanoparticle volume concentration boundary layer thickness is reduced. The influence of concentration slip parameter (β) on concentration profiles is discussed in Fig. 13. From this figure, it is observed that, the concentration profiles are decreasing with increasing of concentration slip parameter (β).

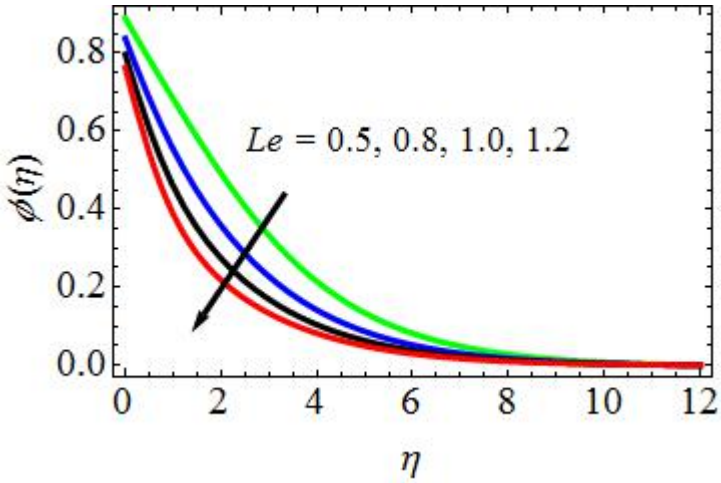

Fig. 12. Effect of *Le* on concentration profiles

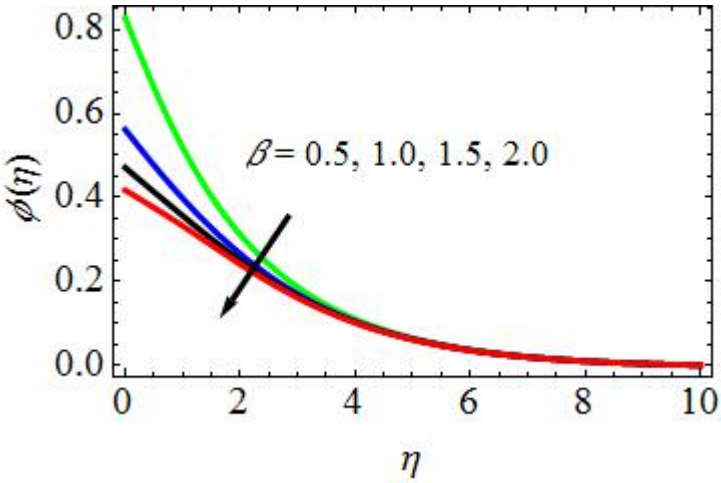

Fig. 13. Effect of β on concentration profiles

Table-2.: Numerical values of Skin-friction coefficient for variations of M^2, λ, δ, β, Pr, *R*, *Nb*, *Nt* and *Le*

M^2	λ	δ	β	Pr	*R*	*Nb*	*Nt*	*Le*	*Cf*
0.5	0.5	0.5	0.5	0.71	0.5	0.1	0.1	0.5	1.302250126659855
0.8									1.263887484512693
1.0									1.229301254661478
	1.0								1.278211660188964
	1.5								1.259667845132408

ISSN: 2366-1313

1.0						1.273200415887325
1.5						1.254111021568717
	1.0					1.279220467820154
	1.5					1.253655487201809
		1.0				1.269200135584126
		3.0				1.249801112145769
			0.9			1.278500120322645
			1.2			1.259660321147688
				0.3		1.283011620248792
				0.5		1.269001248932565
					0.5	1.335001248876019
					0.8	1.354478201265863
						0.8 1.278015039821465
						1.0 1.258221021544885

➔ Table-2 shows the numerical values of Skin-friction coefficient for variations in values of the engineering parameters such as, M^2, λ, δ, β, Pr, R, Nb, Nt and Le. From this table, it is observed that the Skin-friction coefficient is increasing with rising values of Nt, while it is decreasing with increasing values of M^2, λ, δ, β, Pr, R, Nb and Le.

➔ The numerical values of rate of heat transfer coefficient in terms of Nusselt number are displayed in Table-3 for different values of δ, Pr, R, Nb and Nt. The rate of heat transfer coefficient is gradually rising with increasing values of Nb and Nt, while the reverse effect is observed in increasing values of δ, Pr and R.

➔ The effects of β, Nb, Nt and Le on rate of mass transfer coefficient or in terms Sherwood number coefficient are discussed in Table-4. From this table, it is observed that the rate of mass transfer coefficient is decreasing with increasing values of Nb, β and Le, while it increases with increasing values of Nt.

Table-3.: Numerical values of rate of heat transfer coefficient for variations of δ, Pr, R, Nb and Nt

Pr	δ	Nb	Nt	R	Nu
0.71	0.5	0.1	0.1	0.5	0.652201125689522
1.00					0.608441210012564
3.00					0.586330114784196
	1.0				0.628774120634401
	1.5				0.598770215564267
		0.3			0.689220144774326
		0.5			0.705532011989843
			0.5		0.698330214755232
			0.8		0.718551510001423
				0.9	0.604410288723154
				1.2	0.578333144789987

ISSN: 2366-1313

Table-4.: Numerical values of rate of mass transfer coefficient for variations of β, *Nb*, *Nt* and *Le*

B	*Nb*	*Nt*	*Le*	*Sh*
0.5	0.1	0.1	0.5	0.489333026158853
1.0				0.458332695410247
1.5				0.427112267598485
	0.3			0.450211875549321
	0.5			0.427602231058944
		0.3		0.526300189322139
		0.5		0.547660218843097
			0.8	0.446201578459955
			1.0	0.418832056677693

6. Conclusions:

In this current research work, Runge-Kutta method is applied for the numerical solutions of viscous, incompressible, electrically conducting, boundary layer nanofluid flow towards a non-linearly stretching sheet with Thermal radiation, Thermophoresis, Magnetic field, Multiple slips and Brownian motion effects have been calculated. The effects of the various physical engineering parameters M^2, λ, δ, β, Pr, *R*, *Nb*, *Nt* and *Le* on-flow field variables such as velocity, temperature and concentration profiles. Also, the numerical values of Skin-friction coefficient, Nusselt number and Sherwood number displayed in tabular forms. From this research examination, the important findings are:

- ✓ The velocity profiles are decreasing with increasing of M^2 and λ.
- ✓ Also, the Skin-friction coefficient are decreasing with increasing of values of M^2, λ, δ, β, Pr, *R*, *Nb* and *Le*.
- ✓ As the rising values of *Nb* and *Nt*, the temperature profiles are increasing while the reverse effect is observed in increasing values of δ, Pr and *R*.
- ✓ The rate of heat transfer coefficient is gradually rising with increasing values of *Nb* and *Nt*, while the reverse effect is observed in increasing values of δ, Pr and *R*.
- ✓ The concentration profiles are decreasing with increasing values of *Nb*, β and *Le*, while it increasing with increasing values of *Nt*.
- ✓ The rate of mass transfer coefficient is reducing with rising values of *Nb*, β and *Le*, while it rising with growing values of *Nt*.
- ✓ Finally, the present obtained results are compared with the previously published research work done by Wang [31], Reddy Gorla and Sidawi [32], Khan and Pop [33], and Makinde and Aziz [34] for program code validation.

References:

1. B. Tamilzharasan, S. Karthikeyan, M.K. Kaabar, M. Yavuz, F. Özköse, Magneto mixed convection of Williamson nanofluid flow through a double stratified porous medium in attendance of activation energy, Math. Comput. Appl., 27 (3) (2022), p. 46.
2. M. Bilal, Micropolar flow of EMHD nanofluid with nonlinear thermal radiation and slip effects, Alex. Eng. J., 59 (2) (2020), pp. 965-976.

ISSN: 2366-1313

3. K. G. Kumar, E. H. B. Hani, M. E. H. Assad, M. Rahimi-Gorji, S. Nadeem, A novel approach for investigation of heat transfer enhancement with ferromagnetic hybrid nanofluid by considering solar radiation, Microsyst. Technol., 27 (1) (2021), pp. 97-104.
4. J. Raza, F. Mebarek-Oudina, P. Ram, S. Sharma, MHD flow of non-Newtonian molybdenum disulfide nanofluid in a converging/diverging channel with Rosseland radiation, Trans. Tech. Publ. Defect Diffusion Forum, 401 (2020), pp. 92-106.
5. M. M. Nandeppanavar, M. Subhas Abel, M. C. Kemparaju, Stagnation point flow, heat and mass transfer of MHD nanofluid due to porous stretching sheet through porous media with effect of thermal radiation, Journal of Nanofluids, 6 (1) (2017), pp. 38-47.
6. P. Sreedevi, P. Sudarsana Reddy, A. Chamkha, Heat and mass transfer analysis of unsteady hybrid nanofluid flow over a stretching sheet with thermal radiation, SN Appl. Sci., 2 (7) (2020), 10.1007/s42452-020-3011-x.
7. Y. M. Chu, B. M. Shankaralingappa, B. J. Gireesha, F. Alzahrani, M. I. Khan, S. U. Khan, Combined impact of Cattaneo-Christov double diffusion and radiative heat flux on bio-convective flow of Maxwell liquid configured by a stretched nano-material surface, Appl. Math. Comput., 419 (2022), Article 126883.
8. F. S. A. Mubaddel, U. Farooq, K. A. Khaled, S. Hussain, S. U. Khan, M. O. Aijaz, M. R. Gorji, H. Waqas, Double stratified analysis for bioconvection radiative flow of Sisko nanofluid with generalized heat/mass fluxes Phys. Scripta, 96 (2021), Article 055004.
9. M. Azam, Bioconvection and nonlinear thermal extrusion in development of chemically reactive Sutterby nano-material due to gyrotactic microorganisms, Int. Commun. Heat Mass Tran., 130 (2022), Article 105820.
10. M. Azam, A. Shakoor, H. F. Rasool, M. Khan, Numerical simulation for solar energy aspects on unsteady convective flow of MHD Cross nanofluid: a revised approach, Int. J. Heat Mass Tran., 131 (2019), pp. 495-505.
11. M. G. Reddy, S. Rani, K. G. Kumar, A. H. Seikh, M. R. Gorji, E. S. M. Sherif, Transverse magnetic flow over a Reiner-Philippoff nanofluid by considering solar radiation, Mod. Phys. Let., 33 (2019), Article 1950449.
12. M. Sheikholeslami, M. Jafaryar, K. Bateni, D. D. Ganji, Two phase modeling of nanofluid flow in existence of melting heat transfer by means of HAM, Indian J. Phys., 92 (2) (2018), pp. 205-214.
13. Q. M. Al-Mdallal, N. Indumathi, B. Ganga, A. A. Hakeem, Marangoni radiative effects of hybrid-nanofluids flow past a permeable surface with inclined magnetic field, Case Studies in Thermal Engineering., 17 (2020), Article 100571.
14. S. S. Ghadikolaei, K. Hosseinzadeh, M. Hatami, D. D. Ganji, M. Armin, Investigation for squeezing flow of ethylene glycol ($C_2H_6O_2$) carbon nanotubes (CNTs) in rotating stretching channel with nonlinear thermal radiation, J. Mol. Liq., 263 (2018), pp. 10-21.
15. S. S. Ghadikolaei, K. Hosseinzadeh, D. D. Ganji, Investigation on three-dimensional squeezing flow of mixture base fluid (ethylene glycol-water) suspended by hybrid nanoparticle (Fe_3O_4-Ag) dependent on shape factor, J. Mol. Liq., 262 (2018), pp. 376-388.
16. M. Sheikholeslami, M. Shamlooei, Fe3O4-H2O nanofluid natural convection in presence of thermal radiation, Int. J. Hydrogen Energy, 42 (2017), pp. 5708-5718.

ISSN: 2366-1313

17. D. Pal, G. Mandal, Thermal radiation and MHD effects on boundary layer flow of micropolar nanofluid past a stretching sheet with non-uniform heat source/sink, Int. J. Mech. Sci., 126 (2017), pp. 308-318.
18. M. Nayak, N. S. Akbar, V. Pandey, Z. H. Khan, D. Tripathi, 3D free convective MHD flow of nanofluid over permeable linear stretching sheet with thermal radiation, Powder Technol., 315 (2017), pp. 205-215.
19. T. Hayat, M. Rashid, M. Imtiaz, A. Alsaedi, MHD effects on a thermo-solutal stratified nanofluid flow on an exponentially radiating stretching sheet, J. Appl. Mech. Tech. Phys., 58 (2017), pp. 214-223.
20. M. Sheikholeslami, S. Shehzad, Thermal radiation of ferrofluid in existence of Lorentz forces considering variable viscosity, Int. J. Heat Mass Transfer, 109 (2017), pp. 82-92.
21. T. Hayat, M. I. Khan, M. Waqas, A. Alsaedi, M. Farooq, Numerical simulation for melting heat transfer and radiation effects in stagnation point flow of carbon-water nanofluid, Comput. Methods Appl. Mech. Eng., 315 (2017), pp. 1011-1024.
22. T. Hayat, M. Waqas, S. Shehzad, A. Alsaedi, A model of solar radiation and Joule heating in magnetohydrodynamic (MHD) convective flow of thixotropic nanofluid, J. Mol. Liq., 215 (2016), pp. 704-710.
23. M. Sheikholeslami, H. B. Rokni, Magnetic nanofluid natural convection in the presence of thermal radiation considering variable viscosity, Eur. Phys. J. Plus, 132 (2017), p. 238.
24. M. Waqas, M. I. Khan, T. Hayat, A. Alsaedi, Numerical simulation for magneto Carreau nanofluid model with thermal radiation: a revised model, Comput. Methods Appl. Mech. Eng., 324 (2017), pp. 640-653.
25. Yahaya Shagaiya Daniel, Zainal Abdul Aziz, Zuhaila Ismail, Faisal Salah, Effects of thermal radiation, viscous and Joule heating on electrical MHD nanofluid with double stratification, Chin. J. Phys., 55 (3) (2017), pp. 630-651.
26. O. D. Makinde, W. A. Khan, J. R. Culham, MHD variable viscosity reacting flow over a convectively heated plate in a porous medium with thermophoresis and radiative heat transfer, Int. J. Heat Mass Transfer, 93 (2016), pp. 595-604.
27. T. Hayat, M. Waqas, S.A. Shehzad, A. Alsaedi, A model of solar radiation and Joule heating in magnetohydrodynamic (MHD) convective flow of thixotropic nanofluid, J. Mol. Liquids, 215 (2016), pp. 704-710.
28. Utpal Jyoti Das, Free convection heat and mass transfer flow for magnetohydrodynamic chemically reacting and radiating elastico-viscous fluid past a vertical permeable plate with gravity modulation, Int. J. Appl. Comput. Math. (2016), pp. 1-17.
29. Muhammad Ijaz Khan, Muhammad Tamoor, Tasawar Hayat, Ahmed Alsaedi, MHD boundary layer thermal slip flow by nonlinearly stretching cylinder with suction/blowing and radiation, Results Phys., 7 (2017), pp. 1207-1211.
30. S. Arulmozhi, K. Sukkiramathi, S.S. Santra, R. Edwan, U. Fernandez Gamiz, S. Noeiaghdam, Heat and mass transfer analysis of radiative and chemical reactive effects on MHD nanofluid over an infinite moving vertical plate, Results Eng, 14 (Jun. 2022), p. 100394, 10.1016/J.RINENG.2022.100394.
31. C. Y. Wang, Free convection on a vertical stretching surface, ZAMM - J. Appl. Math. Mech./Z. Angew. Math. Mech., 69 (1989) 418-420.

ISSN: 2366-1313

32. R. Reddy Gorla, I. Sidawi, Free convection on a vertical stretching surface with suction and blowing, Appl. Sci. Res. 52 (1994) 247-257.
33. W. A. Khan, I. Pop, Boundary-layer flow of a nanofluid past a stretching sheet, Int. J. Heat Mass Transf. 53 (2010) 2477-2483.
34. O. D. Makinde, A. Aziz, Boundary layer flow of a nanofluid past a stretching sheet with a convective boundary condition, Int. J. Therm. Sci. 50 (2011) 1326-1332.